Kinetic control of dimer structure formation in amyloid fibrillogenesis

Wonmuk Hwang*†, Shuguang Zhang*, Roger D. Kamm†‡, and Martin Karplus§¶‖

*Center for Biomedical Engineering, †Division of Biological Engineering, and ‡Department of Mechanical Engineering, Massachusetts Institute of Technology, Cambridge, MA 02139; §Department of Chemistry and Chemical Biology, Harvard University, Cambridge, MA 02138; and ¶Laboratoire de Chimie Biophysique Institut le Bel, Université Louis Pasteur, 4 Rue Blaise Pascal, 67000 Strasbourg, France

Edited by Alan Fersht, University of Cambridge, Cambridge, United Kingdom, and approved July 19, 2004 (received for review April 13, 2004)

Amyloid fibril formation involves nonfibrillar oligomeric intermediates, which are important as possible cytotoxic species in neurodegenerative diseases. However, their transient nature and polydispersity have made it difficult to identify their formation mechanism or structure. We have investigated the dimerization process, the first step in aggregate formation, by multiple molecular dynamics simulations of five β-sheet-forming peptides. Contrary to the regular β-sheet structure of the amyloid fibril, the dimers exhibit all possible combinations of β-sheets, with an overall preference for antiparallel arrangements. Through statistical analysis of 1,000 dimerization trajectories, each 1 ns in length, we have demonstrated that the observed distribution of dimer configurations is kinetically determined; hydrophobic interactions orient the peptides so as to minimize the solvent accessible surface area, and the dimer structures become trapped in energetically unfavorable conformations. Once the hydrophobic contacts are present, the backbone hydrogen bonds form rapidly by a zipper-like mechanism. The initial nonequilibrium structures formed are stable during the 1-ns simulation time for all five peptides at room temperature. In contrast, at higher temperatures, where rapid equilibration among different configurations occurs, the distribution follows the global energies. The relaxation time of dimers at room temperature was estimated to be longer than the time for diffusional encounters with other oligomers at typical concentrations. These results suggest that kinetic trapping could play a role in the structural evolution of early aggregates in amyloid fibrillogenesis.

Amyloid fibrils are protein aggregates observed in a variety of diseases (1, 2). They commonly exhibit a "cross-β" structure, in which the β-sheet backbone runs perpendicular to the fibril axis, and a backbone hydrogen bond network runs parallel to it (1). It is known that many proteins, including those with no known pathogenic role, can form amyloid fibrils under appropriate conditions (3). Certain synthetic peptides can also self-assemble into similar β-sheet fibers (4), which can be used as a model system for amyloid fibrillogenesis. These self-assembling peptides have also shown promise as biomaterials in tissue engineering (5, 6).

Amyloid fibrillogenesis is a multistage process (7, 8) with a variety of intermediate structures, appearing in different fiber-forming systems; they include α-helices (9), globules (10, 11), toroids (12, 13), and helical ribbons (14). Some of these small oligomeric aggregates have been suggested to be the cytotoxic species in certain neurodegenerative diseases (15, 16). They appear to act as nucleation sites for fibril growth in some cases. Also, several of the aggregates may link together to form a larger protofibril, which is subsequently converted into a fibril by an as yet unknown mechanism (1). The fact that the final amyloid fibrils have essentially the same structure for a wide range of proteins with no apparent sequence homology (1, 3) suggests that there exists a general principle for their assembly. Attempts to explain intermediate formation have been based either on thermodynamic nucleation theories (17, 18) or molecular dynamics (MD) simulations of β-sheet structures using a quasi-equilibrium stability analysis (19–21). However, it is possible that kinetics control the early intermediates, which form metastable structures that are stabilized when larger aggregates are formed. Experimentally, it has recently been suggested that engineered dimeric Alzheimer's β (Aβ) peptides significantly promote the growth of β-sheet fibrils (22). Furthermore, Walsh *et al.* (23) have shown a potential synaptotoxicity of the Aβ dimer *in vivo*. It is thus important to characterize the structure and the formation mechanism of the earliest oligomers.

Here, we focus on the initial dimerization event. By running a large number of MD simulations for a range of small peptides, we show that the observed distribution of dimer conformations follows from their mechanism of formation. Dimerization is initiated by local hydrophobic interactions between two peptides, which drives the system into a configuration that minimizes the solvent accessible surface area (ASA). By running MD simulations at several high temperatures where equilibrium behavior is observed and extrapolating to the room temperature, we show that the relaxation time of the metastable dimers is long enough so that it can participate in larger oligomer formation before relaxation takes place.

The kinetic control of the peptide dimer structures suggests that corresponding features may be found in the formation of larger aggregates, which is consistent with the recent experimental finding by Tcherkasskaya *et al.* (24) that hydrophobic interactions at early stages promote oligomer conformations without the regular β-sheet structure found in the fully formed amyloid fibrils.

Methods

Five β-sheet forming peptides were studied: Aβ_7 (KLVFFAE), Aβ_{7g} (KLVFFAG), K_I (KTVIIE), K_L (KTVLIE), and KFE8 (FKFEFKFE). Aβ_7 is the 16th-22nd residue segment in Aβ. Aβ_{7g} is a mutant where the Glu-22 is replaced by Gly (called the "arctic" mutation), which enhances fibrillization of the Aβ protein (9, 25), although there is no direct evidence for the self-assembling capability of Aβ_{7g}. The other peptides are designed sequences used in the study of fibril formation and peptide self-assembly. Aβ_7, K_I, and KFE8 form antiparallel β-sheet structures (26–28), whereas K_L forms β-sheet aggregates but not fibrils (26). Several peptides were studied to determine sequence-independent characteristics of the dimerization process, because, as already mentioned, many different proteins and peptides can form amyloid fibrils (23, 29).

For simulation, we used CHARMM (30) version 29b1, and used the ACE2 module (31) of CHARMM as a continuum solvent model for the aqueous environment (*Supporting Text*, which is published as supporting information on the PNAS web site). All peptides were acetylated and amidated at N and C termini. For

This paper was submitted directly (Track II) to the PNAS office.

Abbreviations: Aβ, Alzheimer's β; ASA, accessible surface area; Ainv, antiparallel inverted; Aregl, antiparallel regular left-facing; Aregr, antiparallel regular right-facing; MD, molecular dynamics; Pinvl, parallel inverted left-facing; Pinvr, parallel inverted right-facing; Preg, parallel regular.

‖To whom correspondence should be addressed. E-mail: marci@tammy.harvard.edu.

www.pnas.org/cgi/doi/10.1073/pnas.0402634101

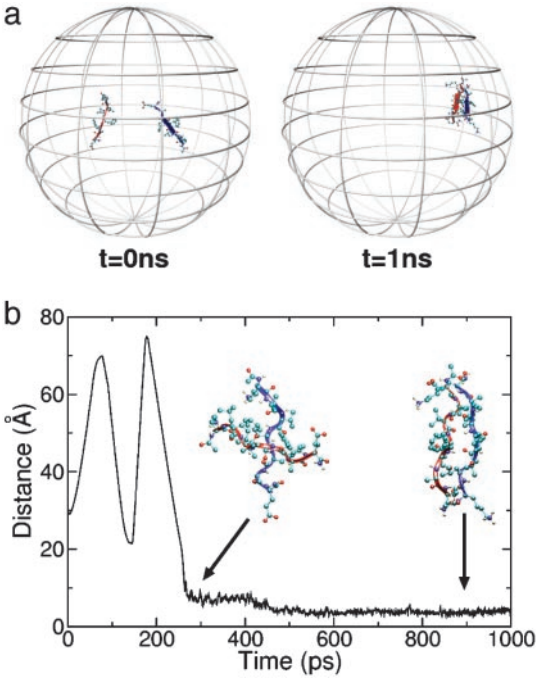

Fig. 1. A sample run of the peptide Aβ_7. (*a*) Initial and final configurations. Framed sphere (45-Å radius) denotes the reflecting boundary. (*b*) Center of mass distance between the peptides versus time. The three extrema before 250 ps correspond to two reflections from the boundary and a collision without coalescence. The configuration at the initial stage of dimerization and the quasi-stable structure after dimerization are marked by arrows.

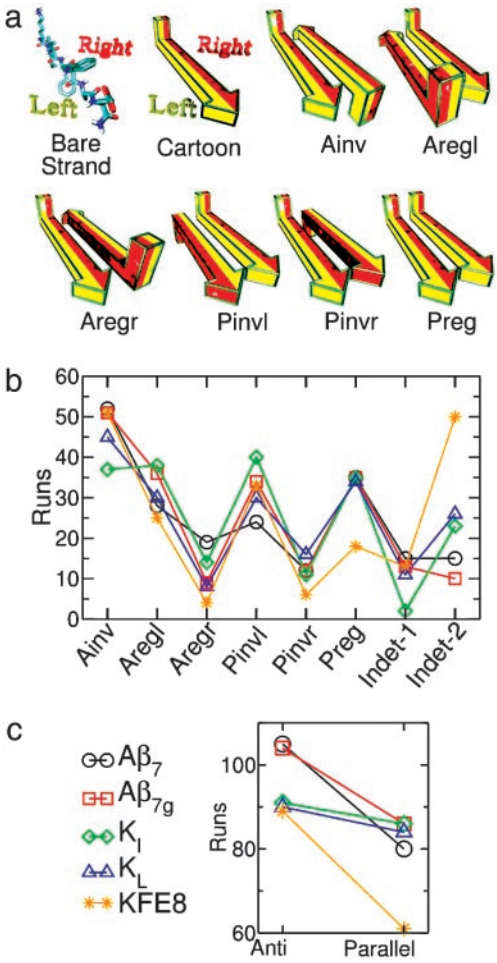

Fig. 2. Dimer structures and their distribution. (*a*) The six possible β-sheet dimers. ''Bare Strand'' and ''Cartoon'' define the left (yellow) and the right (red) sides of a peptide. The arrow's tail is bent in the direction of the first side chain at the N terminus. The dimer structures are named in the following manner: A/P, antiparallel/parallel; inv/reg, first side chains pointing in the opposite (inverted)/the same (regular) directions, distinguished by the tails; l/r, backbone hydrogen bonds formed by using left/right faces of the peptides. (*b*) Distribution of the six possible dimers. Indet-1, antiparallel/parallel can be determined, but further categorization cannot be made because of dihedral transitions that rendered left or right sides of a peptide ill-defined. Indet-2, the peptides have not established definite backbone hydrogen bonds within the simulation time. (*c*) Total number of runs having antiparallel/parallel configurations.

K_I and K_L, the Glu residue was protonated to accommodate for low pH condition at which the experiment was performed (26). To generate a dimerization trajectory, we first ran a single-peptide simulation at 298 K for 1 ns to obtain an average monomer structure. Two such peptides were placed 30 Å apart in random orientations. The system was enclosed by a reflecting sphere of diameter 90 Å (this corresponds to a concentration of 8.7 mM, which is only an order of magnitude larger than the highest concentration used in ref. 26) (Fig. 1*a*; see also *Supporting Text*). Nose–Hoover dynamics (32) at 298 K was run for 1 ns. For the slightly longer peptide KFE8, the initial distance between the peptides was 40 Å and the sphere diameter was 110 Å. The integration time step was 1 fs, and coordinates were saved every 0.5 ps. Two hundred dimerization simulations, each 1 ns in length, were performed for each of the five peptides, for a total simulation time of 1 μs. Depending on the sequence and the trajectory, each simulation took 3–9 h on a 1.7- to 1.8-GHz Intel Xeon CPU in a 16-processor Beowulf cluster.

Hydrogen Bonds and ASA. Backbone hydrogen bonds were identified based on a cutoff of the N—H···O angle at 110° and the H···O distance cutoff of 2.4 Å (33), and the ASA of hydrophobic side chains was calculated by using a probe sphere of radius 1.4 Å for Ala, Phe, Ile, Leu, Val, and Thr (except the -OH group).

In a given dimerization trajectory, the distances between backbone H and O pairs that form hydrogen bonds in the dimer and the ASA of hydrophobic side chains were followed over time (see Fig. 3 *b* and *c*). Algorithms for identifying the hydrogen bond formation and hydrophobic clustering times are explained in *Supporting Text*. Our algorithm failed to identify the hydrogen bond formation time for <1% of the total number of identified hydrogen bonds. Because the ASA data are noisier and there is no well defined cutoff for hydrophobic docking as in the case for hydrogen bonds, the ASAs of many trajectories did not have identifiable docking times. Percentages of runs where the algorithm failed to identify any of the ASA docking events were: 6% (Aβ_7), 2% (Aβ_{7g}), 19.5% (K_I), 10% (K_L), and 31.5% (KFE8).

Equilibrium Simulations. To probe the properties of individual dimers, we have run additional MD simulations starting from preformed dimers. The system was heated from 98 K to 298 K for 20 ps, equilibrated at 298 K for 1 ns, followed by the production run for 5 ns. The integration time step was 2 fs.

For the simulation of Aβ_7 at high temperatures, each of the six preformed dimers in Fig. 2*a* was put in a reflecting sphere of diameter 60 Å, and Nose–Hoover dynamics was performed for 80 ns, totaling 480 ns at each temperature tested: 450, 475, 483, 492, and 500 K. The coordinates were saved every 5 ps. Such high temperatures were used to ensure good sampling between different configurations within the simulation time. The measured energy includes internal and nonbonded terms, as well as

the hydrophobic energy and the solvation free energy from the ACE2 potential. ΔE_{tot} in Fig. 4*b* is the difference between the dimer energy and twice the monomer energy. Simulations were performed in parallel on two 1.70GHz IBM POWER4+ CPUs in a 32-processor p655 machine, and took ≈600 h of computer time for each temperature.

At high temperatures, the system switches between different dimer states (see Fig. 5*a*; see Fig. 2*a* for the definitions of dimer states). Interruptions by the indeterminate state correspond to the unsuccessful attempt of the system to escape from a dimer state. Likewise, a dimer persisting for <10 ps was regarded as transient, and was not counted as a transition event. The transition time, defined as the elapsed time from the formation of a dimer to the transition into the next, thus includes short interruptions and transient periods, as in Fig. 5*a*. On the other hand, the average lifetime of a dimer (see Fig. 4*d*) is based on the uninterrupted duration. For example, in Fig. 5*a*, there are four uninterrupted parallel inverted left-facing (Pinvl) states, though all of them belong to one Pinvl → antiparallel inverted (Ainv) event.

The overall transition time τ was calculated over all of the transition events. In Fig. 5*c*, the average activation energy ΔE_a between dimers was calculated by applying the Arrhenius equation $k = k_0 \exp(-\Delta E_a/k_B T)$, where $k \equiv 1/\tau$ is the transition rate, k_0 is the "free" transition rate at infinite temperature, ΔE_a is the activation energy, k_B is the Boltzmann constant, and T is the temperature. The slope of the linear fits in Fig. 5*c* therefore corresponds to $\Delta E_a/k_B$.

Results

In the simulation of dimerization, the two peptides move within a reflecting sphere (Fig. 1*a*), colliding with the wall and each other until a quasi-stable β-sheet dimer forms (Movie 1, which is published as supporting information on the PNAS web site). An aim of this study is to determine the relationship between the structures that occur in the initial formation of the dimer and the final quasi-stable structure (marked by arrows in Fig. 1*b*). In the example shown in Fig. 1*b*, the peptides start at a center of mass distance of 30 Å, move apart, and collide with the boundary, are reflected and come together in a repulsive configuration, and are repelled; after colliding again with the boundary, they collide with each other and then coalesce (Movie 1). The dimer structure anneals for ≈150 ps, after which it is stable until the end of the trajectory. Most trajectories are similar to the one described, except that the number of collisions before coalescence varies.

The Observed Dimer Distribution Is Nonrandom. To classify the global features of the dimer structure, we use the scheme shown in Fig. 2*a*, which can be used to categorize the structures found in the 1,000 independent simulations. Most of the simulations gave one of the six dimers shown in Fig. 2*a*, although up to 25% (in the case of the peptide KFE8) were too irregular to classify.

The distribution of the six types of dimers does not correspond to that expected from random dimer formation (Fig. 2*b*). Because Ainv and parallel regular (Preg) formations can use either side of the peptide, they would be expected to occur with twice the probability of left- or right- facing dimers if the dimer formation were purely random; i.e., the six configurations in Fig. 2*a* would have ratios of 2:1:1:1:1:2. Although Ainv and Preg have high probabilities, the distribution differs significantly from the expectation for random dimerization; the average ratios are 2.2:1.46:0.50:1.50:0.53:1.46. The low occurrence of Preg is likely to be due to the fact that it has the side chains with the same charge next to each other, making it electrostatically less favorable. An unexpected finding was the preference for left-facing dimers over right-facing ones by a factor of 2.9. We show below that this asymmetry originates from the interaction between the peptides at the moment of dimerization, not from the energetic preference for left-facing dimers.

In addition to the above, the ratio of antiparallel to parallel dimers for all of the peptides taken together was 1.22. Fig. 2*c* shows that this asymmetry holds for all of the peptides, although there is some variation among them. The preference for antiparallel configurations appears to be due to the electric dipole moment of a peptide. As a test, we ran 4-ns simulations at 360 K with each peptide pair harmonically constrained to keep the center of mass distance between 10 and 16 Å, but left the peptides free to rotate. Based on the angle between the vectors connecting the first and the last Cα atoms, the peptides show a consistent preference for the antiparallel configuration: 60.9% (Aβ_7), 60.2% (Aβ_{7g}), 52.8% (K_I), 53.7% (K_L), and 74.2% (KFE8). For comparison, an electrically neutral variant of Aβ_{7g} (QLVFFAG) was simulated. Its dipole moment is significantly lower than the actual peptides (6.4 Debyes versus 52–100 Debyes measured from the center of geometry) and the simulation showed reduced preference for the antiparallel configuration; it was found to be 52.5%, compared to 60.2% for Aβ_{7g}. Although the preference for an antiparallel configuration is slight at the dimer level, the distinction in fibrils is likely to be cooperative in nature so that the bias could become stronger for more extended β-sheet structures (20, 27). For example, in previous simulations of a β-sheet formed from 40 KFE8 monomers, it was found that an antiparallel β-sheet maintained its structure, whereas a parallel β-sheet did not (27).

Hydrophobic Clustering Precedes Hydrogen Bond Formation. Analysis of the dimerization process, which starts in the illustrated trajectory (Fig. 1*b*) at the first arrow, was performed based on backbone hydrogen bond formation and hydrophobic clustering of the side chains, the two most important interactions in β-sheet formation (34, 35).

Fig. 3*a* shows the time difference, Δt_{hb-hp}, between the initial hydrogen bond formation (hb) and the initial hydrophobic docking (hp), for all of the trajectories for which docking times were determined (*Methods*; see also Figs. 6 and 7, which are published as supporting information on the PNAS web site). The time difference is positive in most runs, demonstrating that dimerization is initiated by hydrophobic contacts and further stabilization is achieved through backbone hydrogen bond formation. This finding is in accord with the results for the well analyzed β-hairpin of protein G (34, 35). In all cases except KFE8, there is a large peak at short (<25 ps) delay times between the two, although longer times do occur. KFE8 has the largest ASA (Fig. 4*a*), which corresponds to a strong interaction between the Phe side chains. This interaction slows down the process of reaching a stationary structure, as indicated by the time required for the formation of hydrogen bonds (see below).

The distances between all backbone NH and OC hydrogen bonding pairs were followed over time (Fig. 3*b*). These distances correspond to the center of mass distance in the trajectory (Fig. 1*b*) until the process of dimerization begins. A statistical analysis of the hydrogen bond formation times (*Methods*) demonstrates that, after the first hydrogen bond, the other bonds form in both directions along the backbone in a "zipper-like" manner (Fig. 3*b Inset*). A small fraction of the runs (5–10% of the runs forming dimers, but 35% for KFE8) show more complex behavior; the hydrogen bonds responsible for the nonzipper pattern break, followed by zipper formation. The average times between formation of successive hydrogen bonds are very similar [49.7 ps (Aβ_7), 40.0 ps (Aβ_{7g}), 36.0 ps (K_I), and 44.7 ps (K_L)], except for KFE8, which takes 108.5 ps.

Hydrophobic clustering, as determined by the reduction in the ASA, is illustrated in Fig. 3*c* (*Methods*). Because the solvent exposure of hydrophobic side chains is maximal when the two peptides are separated, the initial hydrophobic contact results in

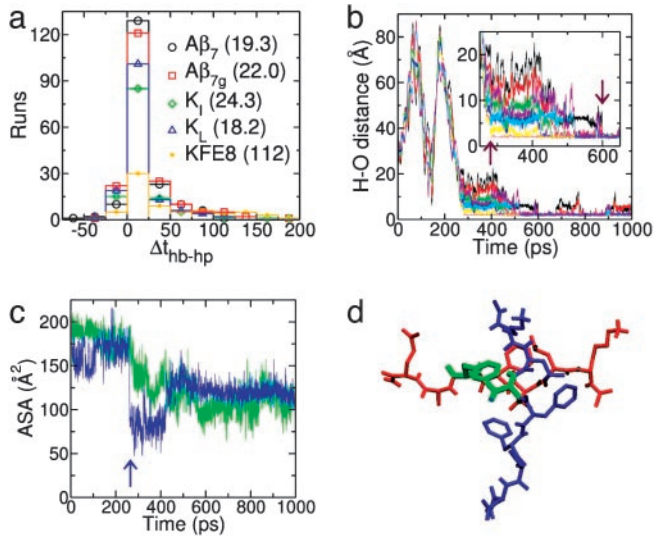

Fig. 3. The dimerization process. (*a*) Distribution of the time difference between initial hydrogen bond formation (hb) and initial hydrophobic clustering (hp). Numbers in parentheses are averages (in picoseconds). (*b*) Distances between backbone H—O pairs of the run in Fig. 1 that form hydrogen bonds; each color indicates one of the H—O pairs. (*Inset*) A magnified view during the period of structured dimer formation. Arrows indicate identified times of the first (280.5 ps) and last (599.5 ps) hydrogen bond formation. (*c*) For the same run, sample ASA trajectories of two Phe side chains. Arrow indicates identified initial hydrophobic clustering time (265 ps). Note that the other ASA trajectory does not have a sharp transition. (*d*) Configuration at the point marked by the arrow in *c*. The side chains engaged in the initial hydrophobic contact are emphasized by thick green bonds.

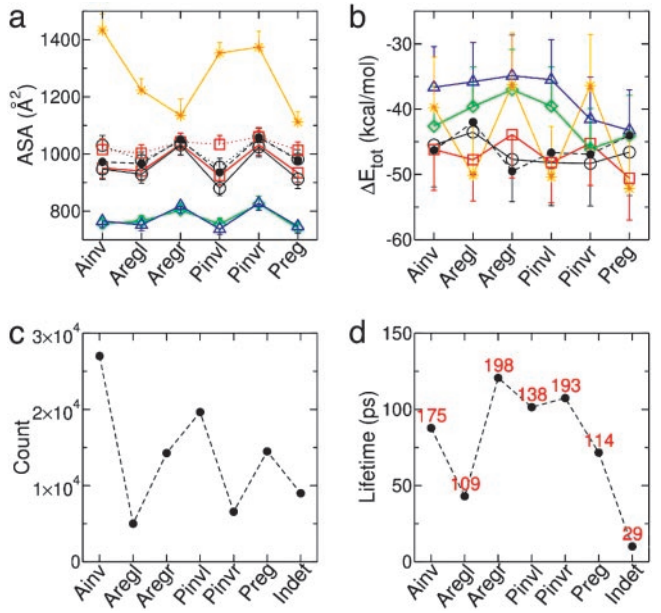

Fig. 4. Equilibrium properties of dimers. Average ASA (*a*) and energy (*b*) are shown (see *Methods*). Symbols and color codes are the same as in Fig. 3*a*. All data are at 298 K except for Aβ_7, which is at 475 K (solid circle with dashed line). For Aβ_7 and Aβ_{7g}, the ASA is calculated both with Ala (dotted line), and without Ala (solid/dashed lines); see text. (*c* and *d*) Behavior of the Aβ_7 dimer at 475 K. ''Indet'' includes both Indet-1 and -2. (*c*) Number of time points (recorded in 5-ps intervals) in a given configuration. (*d*) Average lifetime. Annotated values are standard deviations. Profiles at other high temperatures tested behave similarly.

a sharp decrease in the ASA; this point was used in determining the time delays presented in Fig. 3*a*. After the initial drop, the decrease can be more gradual or an increase can occur. In Fig. 3*c*, the ASA with the identified clustering time increases at ≈500 ps. This adjustment would be required for proper backbone hydrogen bond formation. In many cases, the peptides initially come together with their hydrophobic side chains facing each other (Fig. 3*d*). After forming backbone hydrogen bonds, there can still be an adjustment of the geometry to optimize them, resulting in an increase of the ASA (Fig. 8, which is published as supporting information on the PNAS web site).

Origin of the Preference for Left-Facing Configurations. The fact that dimer formation is initiated by hydrophobic clustering suggests that it may be responsible for the preference for the left-facing configurations. To test this hypothesis, we investigated equilibrium-like properties of individual dimer configurations by running separate 5-ns simulations at 298 K on each of the preformed dimers (*Methods*). During the run, the structures persisted except for antiparallel regular right-facing (Aregr) of KFE8, which became disrupted after 1 ns. The ASA of the left-facing configurations is consistently less than that of the right-facing configurations, whereas the energy profiles do not follow the dimer configurational distribution (Fig. 4 *a* and *b*). The left–right asymmetry in ASA is enhanced when ASA does not include the contribution from Ala, which is least frequently involved in the initial hydrophobic clustering; Ala occurs for only 4.3% (Aβ_7) and 5.6% (Aβ_{7g}) of the identified initial hydrophobic docking events (Fig. 4*a*). This finding suggests that the initial hydrophobic interaction rotates the peptides to minimize the ASA, rather than the overall energy (Fig. 8).

The KFE8 Exception and Equilibrium Behavior. For KFE8, the ASA profile lacks strong left–right asymmetry. Its much slower dimerization makes possible sampling of a greater range of conformations than for the other peptides, so that the overall energy is more important than the hydrophobic interaction in KFE8. At higher temperatures, more rapid sampling is possible and behavior similar to that of KFE8 is expected for the other peptides. To test this, the Aβ_7 dimers were simulated for 480 ns at five different temperatures between 450 and 500 K (*Methods*). The energy and the ASA profiles do not differ much from those at 298 K (open and solid circles in Fig. 4 *a* and *b*). However, the resultant distribution of conformations follows the energy profile (Fig. 4 *c* and *d*), with the lowest energy configuration, Aregr, occurring most frequently. During the 480-ns run, complete dissociation into two separate monomers occurred between 4 (450 K) and 77 (500 K) times, with the average separation times varying between 94.0 ps (450 K) and 54.8 ps (500 K). Thus, dissociation is a relatively rare event and the dimers generally change their structure while remaining aggregated; i.e., the initial contact configurations of the monomers plays a negligible role in the equilibrium case.

Estimating the Relaxation Time of the Dimer. At higher temperatures, the relaxation time is within the range of the simulations, and we extrapolated the results to room temperature to obtain information about the room temperature relaxation time of dimers. Although the initial (metastable) dimer structures were stable up to 5 ns at room temperature, an isolated dimer would eventually relax to its equilibrium structure. However, if the dimer encounters other oligomer species before it relaxes, the initial conformation would play an important role in determining the structures of the oligomers. This is what is meant by kinetic control.

Fig. 5*a* describes a typical transition event for the Aβ_7 dimer. The number of transitions observed during 480 ns at each temperature is shown in Fig. 5*b*. The number of transitions at 492

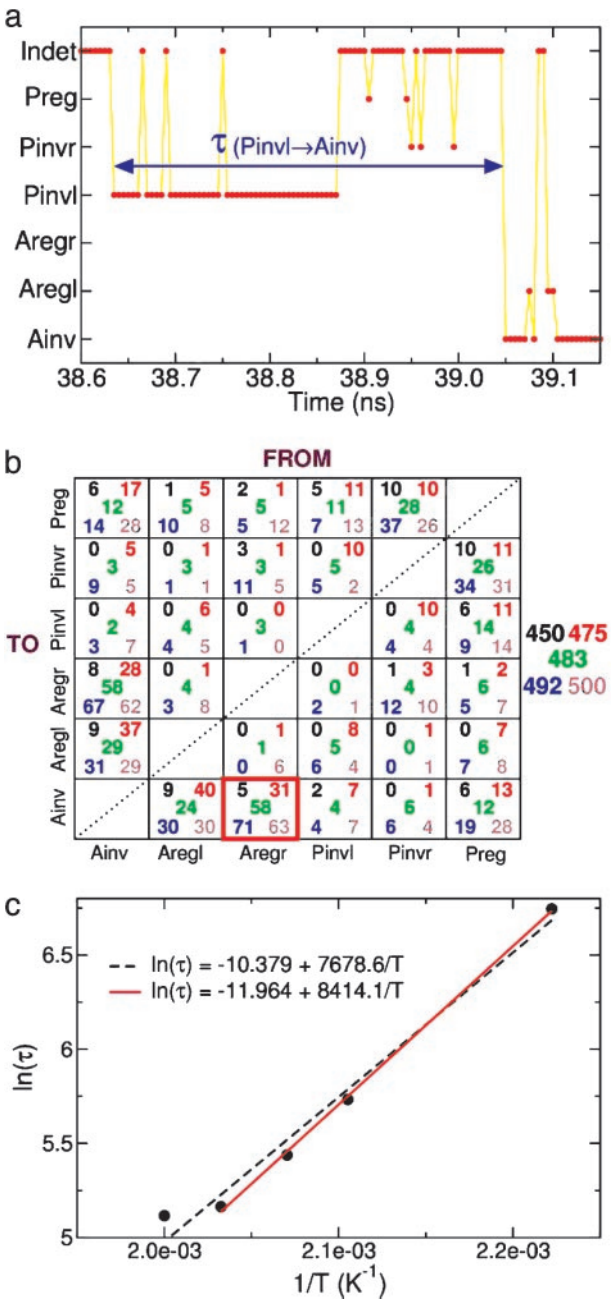

Fig. 5. Transition between dimer states of Aβ_7. (*a*) An example trajectory at 483 K, illustrating the definition of the transition time (Fig. 9). ''Indet'' includes both Indet-1 and -2. Preg and Pinvr during 38.9–39.0 ns lasted <10 ps, so they were ignored (*Methods*). (*b*) Number of transition events, color-coded and positioned according to temperatures noted on the right side. Each cell represents a transition from the dimer marked on the x-axis to the one on the y-axis. For example, the red box corresponds to Aregr → Ainv. (*c*) Plot of ln(τ) versus 1/T. Solid line, linear fit excluding the point at 500 K; dashed line, fit with all of the data.

and 500 K is ≈1.8 times that at 450 and 475 K. Transitions to and from Ainv or Preg are more frequent than those between left- and right-facing dimers. The most abundant ones are Ainv ↔ (Aregl, Aregr) and Preg ↔ (Pinvl,Pinvr). Because Ainv and Preg use both the left and the right faces of the peptides, a rotation along the major axis of one of the peptides is sufficient for the transition into left- or right-facing dimers. On the other hand, both of the peptides in a left (right)-facing dimer must rotate to form a right (left)-facing dimer. The antiparallel ↔ parallel transition is also difficult because a peptide has to rotate 180° about the axis perpendicular to the β-sheet, so the least likely transitions are those such as antiparallel regular left-facing (Aregl) ↔ parallel inverted right-facing (Pinvr). In this sense, Ainv and Preg act as the "gateways" in dimer formation as they form abundantly when two separate peptides initially dimerize (Fig. 2*b*), and also mediate transitions to and from the other dimer states.

The symmetry in Fig. 5*b* along the diagonal (dotted line) shows that forward and backward transitions between two states occur with nearly equal frequency, indicating detailed balance (36), so that the simulations were long enough to exhibit equilibrium behavior. However, the average transition time between dimers is not symmetric (Fig. 9, which is published as supporting information on the PNAS web site) because of the relative stability of dimers (see Fig. 4*b*). It also does not have a strong monotonic dependence on temperature, with a large standard deviation. Apart from the sampling error, this is presumably because the transition pathway between two dimers on the energy landscape is not well defined. However, the overall transition time τ shows a monotonic decrease with temperature, as it includes a large number of transition events. The activation energy calculated from Fig. 5*c* is ΔE_a = 15.3–16.7 kcal/mol (*Methods*), ≈30% of the free energy of dimerization, ΔE_{tot} (Fig. 4*b*). From the linear fits, we estimate τ at 298 K to be 4.8–11.7 μs. Considering that the simulations were performed in zero-viscosity continuum solvent, τ is expected to be significantly longer in actual solvent. A related implicit solvent model (19) found that protein folding occurred on a time scale nearly two orders of magnitude faster than experiment. This result suggests a millisecond time scale for τ.

We can compare τ with the diffusion time scale of dimers. At a typical concentration of 1 mM (26, 28), if one assumes that all monomers in the solution initially form a dimer, the dimer concentration is 0.5 mM, giving a mean interdimer distance of 150 Å. Using the radius of gyration of a dimer, r_g = 8.15 Å, its diffusion coefficient calculated from the Stokes–Einstein relation is $D = k_B T/12\pi\eta r_g = 1.5 \times 10^{-10}$(m^2/s) ($\eta = 8.94 \times 10^{-4}$ N·s/m^2: dynamic viscosity of water). The diffusion time for the distance l = 150 Å is then $t_D = l^2/6D \approx 0.25$ (μs). Even if we use 0.1 mM as the peptide concentration, t_D = 1.2 μs. Clearly, $t_D < \tau$, and we conclude that the initial dimer structure will interact with other species before it relaxes.

Concluding Discussion. A large number (200 runs of 1-ns duration for each species) of dimerization simulations for several peptides were performed to obtain statistically meaningful results. Of particular interest is the finding of kinetically trapped dimers with a slow relaxation time, suggesting that they may be involved in the structural evolution of oligomers. In explicit solvent, the relaxation is expected to be still longer because of viscosity effects not included in the calculations.

Furthermore, for Aβ_7, preliminary simulations of interactions between a dimer and a monomer and between two dimers showed that kinetic control persists and the preference for antiparallel, left-facing binding is preserved (Fig. 10, which is published as supporting information on the PNAS web site). In addition to oligomerization, because an antiparallel β-sheet consists of alternation between the Aregl and Aregr binding modes, our finding should apply to the fibril growth stage. The fact that Aregl is easier to form, but has higher energy than Aregr, would cause uneven fibril growth rates depending on which side of the peptide is exposed.

Although it has not been possible to probe the kinetics of dimer and small oligomer formation experimentally, we expect the relaxation time to increase as the aggregate grows in size and for longer peptide sequences. This would mean that a kinetically

trapped state could be dominant for larger structures. Circumstantial evidence for this can be found in the existence of intermediates of various nonfibrillar morphologies (9–14, 37). From a kinetic point of view, they occur because they are easier to form, not because they are energetically more stable. Moreover, amyloid fibrils do not easily denature at temperatures up to 90°C (4, 38). Thus, under physiological conditions, they may be trapped in local minima, a necessary condition for kinetic control.

We did not observe any fundamental differences in the dimer formation behavior between fibril forming and nonforming peptides. One possibility, consistent with the proposal by Lomakin *et al.* (39), is that the distinction between fibril forming and nonforming peptides only becomes manifest in larger aggregates. Also, this could be due, in part, to the use of a continuum model for the solvent. One-nanosecond explicit water simulations were performed starting from preformed dimers of $A\beta_7$ (Aregl, Aregr, Pinvl, and Preg) and the fibril nonforming K_L (Aregl, Aregr, and Preg) (data not shown). For $A\beta_7$, Aregl and Aregr were stable, whereas for Pinvl and Preg, the backbone hydrogen bonds near the C terminus broke, even though their identity as Pinvl or Preg persisted until the end of the simulation. On the other hand, for K_L, only Aregr was stable and the other two dimers ended up in indeterminate configurations. For $A\beta_7$, the average ASA of Aregl (971 Å^2) was still less than that of Aregr (1,104 Å^2), consistent with kinetic trapping driven by hydrophobic interactions found with implicit solvent. Obtaining meaningful results with explicit solvent will require longer simulations because the water structural relaxation, which is adiabatic with implicit solvent, is on the same time scale as the peptide motions. Such simulations may become possible in the future with large numbers of processors (i.e., one per grid).

We thank Hilal A. Lashuel for helpful discussions on intermediate structures in amyloid formation. This work was funded in part by the DuPont–MIT Alliance and by Merck through the MIT Computational and Systems Biology Initiative (CSBi). We gratefully acknowledge the generous donation of computers by Intel Corporation. The work at Harvard University (M.K.) was supported in part by a grant from the National Institutes of Health.

1. Rochet, J.-C. & Lansbury, P. T. (2000) *Curr. Opin. Struct. Biol.* **10,** 60–68.
2. Sunde, M., Serpell, L. C., Bartlam, M., Fraser, P. E., Pepys, M. B. & Blake, C. C. F. (1997) *J. Mol. Biol.* **273,** 729–739.
3. Dobson, C. M. (2002) *Nature* **418,** 729–730.
4. Zhang, S., Lockshin, C., Cook, R. & Rich, A. (1994) *Biopolymers* **34,** 663–672.
5. Holmes, T. C., de Lacalle, S., Su, X., Liu, G., Rich, A. & Zhang, S. (2000) *Proc. Natl. Acad. Sci. USA* **97,** 6728–6733.
6. Kisiday, J. D., Jin, M., Kurz, B., Huang, H., Semino, C. E., Zhang, S. & Grodzinsky, A. J. (2002) *Proc. Natl. Acad. Sci. USA* **99,** 9996–10001.
7. Aggeli, A., Nyrkova, I. A., Bell, M., Harding, R., Carrick, L., McLeish, T. C. B., Semenov, A. N. & Boden, N. (2001) *Proc. Natl. Acad. Sci. USA* **98,** 11857–11862.
8. Kelly, J. W. (1998) *Curr. Opin. Struct. Biol.* **8,** 101–106.
9. Kirkitadze, M. D., Condron, M. M. & Teplow, D. B. (2001) *J. Mol. Biol.* **312,** 1103–1119.
10. Conway, K. A., Lee, S.-J., Rochet, J.-C., Ding, T. T., Williamson, R. E. & Lansbury, P. T. (2000) *Proc. Natl. Acad. Sci. USA* **97,** 571–576.
11. Yong, W., Lomakin, A., Kirkitadze, M. D., Teplow, D. B., Chen, S. & Benedek, G. B. (2002) *Proc. Natl. Acad. Sci. USA* **99,** 150–154.
12. Lashuel, H. A., Hartley, D., Petre, B. M., Walz, T. & Lansbury, P. T. (2002) *Nature* **418,** 291.
13. Lashuel, H. A., Petre, B. M., Wall, J., Simon, M., Nowak, R. J., Walz, T. & Lansbury, P. T. (2002) *J. Mol. Biol.* **322,** 1089–1102.
14. Marini, D. M., Hwang, W., Lauffenburger, D. A., Zhang, S. & Kamm, R. D. (2002) *Nano Lett.* **2,** 295–299.
15. Bucciantini, M., Giannoni, E., Chiti, F., Baroni, F., Formigli, L., Zurdo, J., Taddei, N., Ramponi, G., Dobson, C. M. & Stefani, M. (2002) *Nature* **416,** 507–511.
16. Volles, M. J., Lee, S.-J., Rochet, J.-C., Shtilerman, M. D., Ding, T. T., Kessler, J. C. & Lansbury, P. T. (2001) *Biochemistry* **40,** 7812–7819.
17. Lomakin, A., Teplow, D. B., Kirschner, D. A. & Benedek, G. B. (1997) *Proc. Natl. Acad. Sci. USA* **94,** 7942–7947.
18. Perutz, M. F. & Windle, A. H. (2001) *Nature* **412,** 143–144.
19. Gsponer, J., Haberthür, U. & Caflisch, A. (2003) *Proc. Natl. Acad. Sci. USA* **100,** 5154–5159.
20. Klimov, D. K. & Thirumalai, D. (2003) *Structure (London)* **1,** 295–307.
21. Ma, B. & Nussinov, R. (2002) *Protein Sci.* **11,** 2335–2350.
22. Schmechel, A., Zentgraf, H., Scheuermann, S., Fritz, G., Pipkorn, R., Reed, J., Beyreuther, K., Bayer, T. A. & Multhaup, G. (2003) *J. Biol. Chem.* **278,** 35317–35324.
23. Walsh, D. M., Klyubin, I., Fadeeva, J. V., Cullen, W. K., Anwyl, R., Wolfe, M. S., Rowan, M. J. & Selkoe, D. J. (2002) *Nature* **416**, 535–539.
24. Tcherkasskaya, O., Sanders, W., Chynwat, V., Davidson, E. A. & Orser, C. S. (2003) *J. Biomol. Struct. Dyn.* **21,** 353–365.
25. Nilsberth, C., Westlind-Danielsson, A., Eckman, C. B., Condron, M. M., Axelman, K., Forsell, C., Stenh, C., Luthman, J., Teplow, D. B., Younkin, S. G., *et al.* (2001) *Nat. Neurosci.* **4,** 887–893.
26. de la Paz, M. L., Goldie, K., Zurdo, J., Lacroix, E., Dobson, C. M., Hoenger, A. & Serrano, L. (2002) *Proc. Natl. Acad. Sci. USA* **99,** 16052–16957.
27. Hwang, W., Marini, D. M., Kamm, R. D. & Zhang, S. (2003) *J. Chem. Phys.* **118,** 389–397.
28. Balbach, J. J., Ishii, Y., Antzukin, O. N., Leapman, R. D., Rizzo, N. W., Dyda, F., Reed, J. & Tycko, R. (2000) *Biochemistry* **39,** 13748–13759.
29. Chiti, F., Webster, P., Taddei, N., Clark, A., Stefani, M., Ramponi, G. & Dobson, C. M. (1999) *Proc. Natl. Acad. Sci. USA* **96,** 3590–3594.
30. Brooks, B. R., Bruccoleri, R. E., Olafson, B. D., States, D. J., Swaminathan, S. & Karplus, M. (1983) *J. Comput. Chem.* **4,** 187–217.
31. Schaefer, M., Bartels, C., Leclerc, F. & Karplus, M. (2001) *J. Comput. Chem.* **22,** 1857–1879.
32. Hoover, W. G. (1985) *Phys. Rev. A* **31,** 1695–1697.
33. de Loof, H., Nilsson, L. & Rigler, R. (1992) *J. Am. Chem. Soc.* **114,** 4028–4035.
34. Dinner, A. A., Lazardis, T. & Karplus, M. (1999) *Proc. Natl. Acad. Sci. USA* **96,** 9068–9073.
35. Pande, V. S. & Rokhsar, D. S. (1999) *Proc. Natl. Acad. Sci. USA* **96,** 9062–9067.
36. Gardiner, C. W. (1983) *Handbook of Stochastic Methods* (Springer, Berlin).
37. Kowalewski, T. & Holtzman, D. M. (1999) *Proc. Natl. Acad. Sci. USA* **96,** 3688–3693.
38. MacPhee, C. E. & Dobson, C. M. (2000) *J. Mol. Biol.* **297,** 1203–1215.
39. Lomakin, A., Chung, D., Benedek, G. B., Kirschner, D. A. & Teplow, D. B. (1996) *Proc. Natl. Acad. Sci. USA* **93,** 1125–1129.